Supporting Information

"Comprehensive Phase Diagrams of MoS_2 Edge Sites using Dispersion-Corrected DFT Free Energy Calculations"

A.S. Rosen, J.M. Notestein, and R.Q. Snurr.

Corresponding authors:

E-mail: snurr@northwestern.edu

E-mail: j-notestein@northwestern.edu

Excel Sheet and Python Script Documentation

Please refer to the "readme.txt" file for information regarding the Excel sheet, the Python script, and structural data.

DFT Convergence Tests

The kinetic energy cutoff and k-point grid were determined based on a series of energy convergence tests on the MoS_2 simulation unit cell shown in Figure 1 of the main manuscript. All convergence tests were done with a = 3.15 Å, $c/2$ = 6.07 Å, and ζ = 0.129. The experimental values are a = 3.16 Å, $c/2$ = 6.15 Å, and ζ = 0.129.[1] Table S1 shows the absolute energy convergence with regards to the energy cutoff. Based on the results in Table S1, an energy cutoff of 650 eV is sufficiently precise. Table S2 shows the absolute energy with regards to the k-point grid, indicating that a $4 \times 2 \times 2$ k-point grid is appropriate.

Table S1. Convergence test for the kinetic energy cutoff (with a fixed $2 \times 2 \times 2$ k-point grid and 20 Å of total vacuum space per cell).

Energy cutoff (eV)	Absolute energy (eV)
200	-513.6583
300	-521.9575
400	-522.1114
500	-522.1806
600	-522.1996
650	-522.2063
700	-522.2103

Table S2. Convergence test for the Monkhorst-Pack k-point grid (with a fixed 500 eV energy cutoff and 20 Å of total vacuum space per cell).

k-point grid	Absolute energy (eV)
$2 \times 2 \times 2$	-522.1806
$4 \times 2 \times 2$	-522.2555
$6 \times 2 \times 2$	-522.2481
$4 \times 4 \times 2$	-522.2459

Additional DFT Settings

In addition to the DFT details discussed in the Methodology section, the following settings were used. A Monkhorst-Pack $22 \times 22 \times 22$ k-point grid was used to sample the Brillouin zone during the structural optimization of bulk Mo. Spin-polarization was considered for the bulk Mo calculation. The resulting lattice constants were $a = b = c =$ 3.13 Å, $\alpha = \beta = \gamma =$ 90°. The experimental values are $a = b = c =$ 3.14 Å, $\alpha = \beta = \gamma$ = 90° (AMCSD Database Code 0012937).[2] The starting structure for α-sulfur was obtained from the American Mineralogist Crystal Structure Database (AMCSD Database Code 0010057),[2] and a Monkhorst-Pack $4 \times 3 \times 2$ k-point grid was used during the optimization. The resulting lattice constants were a = 10.26 Å, b = 12.71 Å, c = 24.27 Å, $\alpha = \beta = \gamma$ = 90°. The experimental values are a = 10.46 Å, b = 12.87 Å, c = 24.49 Å, $\alpha = \beta = \gamma$ = 90°. All gas-phase molecules were sampled using the Γ-point only, and 20 Å of vacuum space was used in each dimension to prevent spurious self-interactions.

Structural Parameter Optimization

The structure of multilayer hexagonal (2H) MoS_2 has three free parameters to vary: a, $c/2$, and ζ. The a lattice parameter was varied between 3.14 Å and 3.16 Å in intervals of 0.01 Å, the $c/2$ lattice parameter was varied between 5.90 Å and 6.15 Å in intervals of 0.05 Å, and ζ was varied between 0.128 and 0.131 in intervals of 0.001. Since the region surrounding the equilibrium value is quadratic in shape, the data at each ζ value can be fit to a paraboloid of the form $E(a, c/2, \zeta) = p_{00} + p_{10}a + p_{01}(c/2) + p_{20}a^2 + p_{11}a(c/2) + p_{02}(c/2)^2$. The global minimum was found analytically and then used to find the a and $c/2$ values that minimize E at a given ζ. The result of this sampling is visually described in Figure S1.

The paraboloid with the lowest energy minimum should correspond to the minimum energy a, $c/2$, and ζ values for 2H-MoS_2. A plot of the minimum energy for each paraboloid as a function of ζ is shown in Figure S2. From this plot, it is apparent that $\zeta \approx 0.129$ minimizes the energy of the 2H-MoS_2 unit cell. The corresponding a and $c/2$ values that minimize the energy at ζ = 0.129 are approximately 3.15 Å and 6.07 Å, respectively. As such, the equilibrium parameters are determined to be $a \approx 3.15$ Å, $c/2 \approx 6.07$ Å, and $\zeta \approx 0.129$ within the context of the PBE functional and D3(BJ) dispersion correction. To confirm that this result is accurate, total energy calculations were performed in VASP at a = {3.14 Å, 3.15 Å, 3.16 Å}, $c/2$ = {6.06, 6.07, 6.08}, and ζ = {0.128, 0.129, 0.130}. This manual check confirmed the equilibrium values of a, $c/2$, and ζ corresponded to a minimum in the total energy.

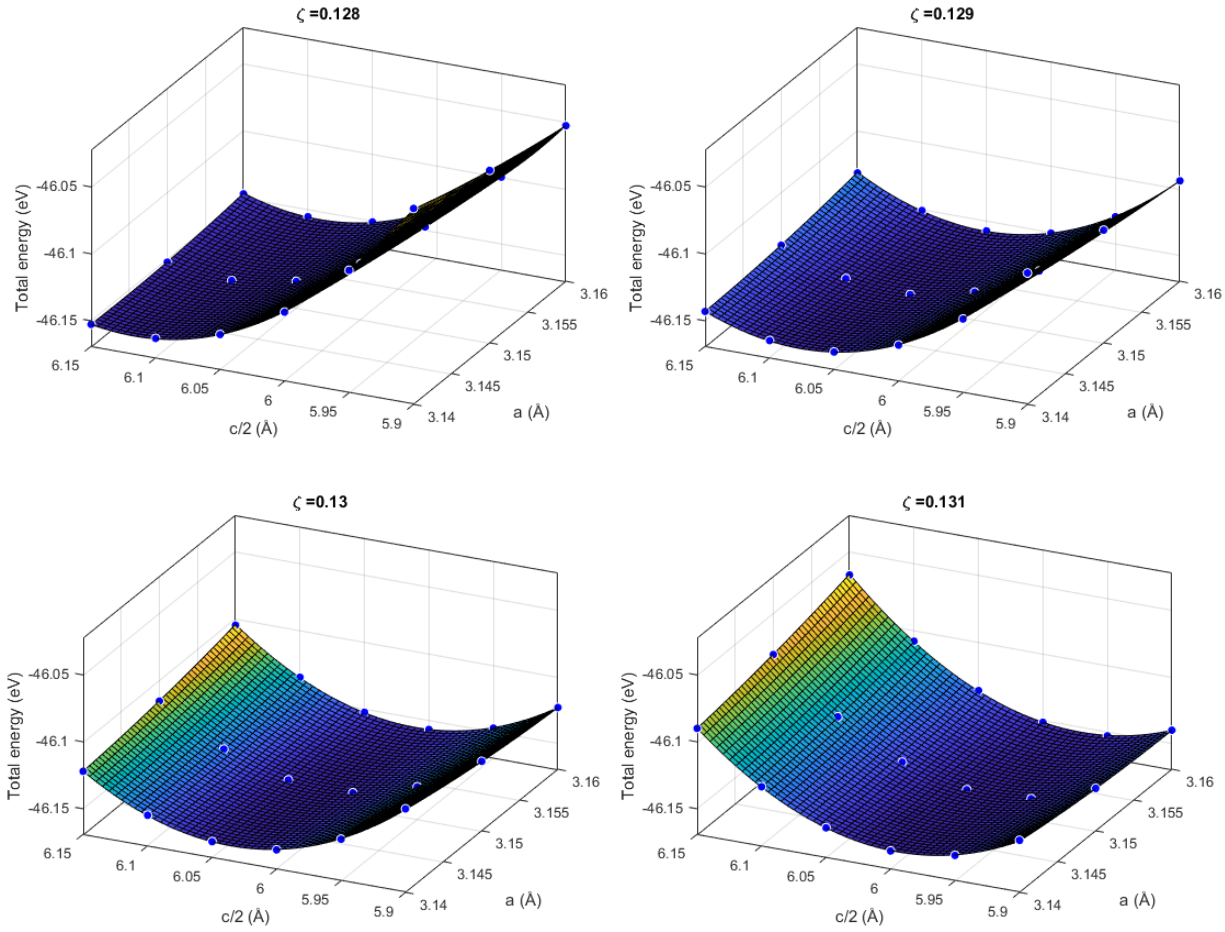

Figure S1. Total energy of bulk MoS_2 as a function of a and $c/2$ at fixed ζ values. The blue markers represent values computed from DFT, and the paraboloid represents the best fit equation.

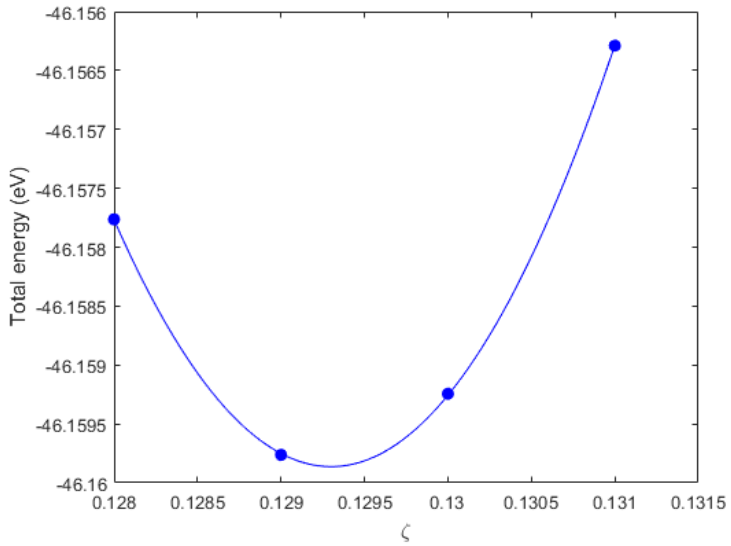

Figure S2. Minimum value of $E(a, c/2, \zeta)$ for the 2H-MoS_2 unit cell as a function of ζ.

Vibrational Mode Assumptions

To justify the assumptions made in the vibrational frequency analysis, we report in Table S3 the value of $F^{\mathrm{vib}}_{\mathrm{MoS}_x\mathrm{H}_y}(T)$ using Equation (6) compared to doing a full vibrational frequency analysis (including the coupled vibrations of all S* and H* atoms). For all tested structures, the error is quite low – far below errors expected from DFT and the harmonic approximation. This is due in part to the fact that the low-frequency modes, which contribute most to the Helmholtz free energy, can be attributed to surface S atoms, whose vibrational modes are explicitly computed for each S-coverage. In addition, it is apparent that the decoupled vibrational mode assumption is quite accurate, as the vibrational modes of S* and H* separately are similar to those obtained from the full, coupled vibrational analysis.

Table S3. Relative error in calculating the vibrational contribution to the Helmholtz free energy, $F^{\mathrm{vib}}_{\mathrm{MoS}_x\mathrm{H}_y}(T)$, for various edge structures as a function of temperature. The (coupled) vibrational frequencies of S* and H*, denoted ν, and the decoupled vibrational frequencies of S* (ν_{S^*}), H* on Mo atoms ($\nu_{\mathrm{H}^*/\mathrm{Mo}}$), and H* on S atoms ($\nu_{\mathrm{S}^*/\mathrm{S}}$) are reported.

					Relative error in $F^{\mathrm{vib}}_{\mathrm{MoS}_x\mathrm{H}_y}$ (eV)		
Edge	ν (cm^{-1})	ν_{S^*} (cm^{-1})	$\nu_{\mathrm{H}^*/\mathrm{Mo}}$ (cm^{-1})	$\nu_{\mathrm{H}^*/\mathrm{S}}$ (cm^{-1})	300 K	650 K	1000 K
Mo-0/33	571, 874, 1193	---	571, 874, 1193	---	0	0	0
Mo-33/33	87, 95, 174, 210, 363, 378, 529, 722, 1039	87, 96, 175, 211, 363, 378	528, 721, 1038	---	0.01	0.01	0.05
Mo-50/33	71, 87, 100, 206, 238, 265, 273, 373, 386, 504, 614, 2555	72, 94, 215, 234, 273, 300, 373, 386, 470	---	486, 594, 2517	-0.003	-0.01	-0.01
Mo-67/67	85, 94, 115, 184, 220, 223, 240, 250, 264, 266, 281, 530, 538, 556, 593, 607, 2544, 2545	115, 192, 222, 237, 246, 255, 272, 279, 295, 464, 467, 531	---	522, 542, 579, 590, 2506, 2507	0.03	0.06	0.09

S-50/33	80, 108, 139, 257, 297, 308, 344, 347, 363, 764, 1093, 1230	82, 108, 142, 257, 298, 309, 345, 349, 364	763, 1092, 1230	---	-0.004	-0.01	-0.01
S-67/67	92, 124, 139, 193, 233, 245, 274, 297, 309, 342, 354, 361, 611, 677, 753, 1039, 1255, 2447	92, 141, 166, 236, 268, 280, 299, 309, 337, 355, 363, 473	751, 1039, 1255	593, 645, 2412	-0.02	-0.04	-0.05
S-100/33	106, 120, 124, 170, 173, 190, 202, 228, 242, 263, 291, 301, 302, 312, 322, 344, 352, 371, 618, 658, 2444	111, 124, 154, 170, 186, 202, 229, 242, 287, 294, 301, 306, 320, 321, 339, 352, 369, 468	---	597, 644, 2409	-0.01	-0.01	-0.01

Comments on Certain Edge Structures

As reported in Table 3, it was found that the lowest energy configuration for $\theta_S = 1$ on the S-edge has uniformly spaced S monomers based on the proposed adsorption sites by Raybaud and coworkers.[3] In prior work by Prodhomme et al.[4] and Hinnemann et al.[5], an alternating sequence of S monomers and dimers was predicted to be more stable than the full monomer configuration, so it is worth investigating this impact of dimers on the S-edge at 100% S-coverage. As shown in Table S4, the full monomer configuration is in fact the most stable structure for multilayer MoS_2 at the PBE-D3(BJ) level of theory considered in the present work. This holds true for both the 3 Mo unit cell considered in this work and the symmetric 4 Mo unit cell considered by Prodhomme and coworkers.[4] Whereas Prodhomme et al. predict that the alternating monomer/dimer configuration is more stable than the monomer configuration by 0.99 eV, we find it to be less stable by 0.17 eV. This is due to the fact that the MoS_2 model in the present work is a multilayer structure, whereas the aforementioned work used an infinite stripe model consisting of a single MoS_2 monolayer. To confirm that this is the cause, we considered an infinite stripe model of the S-edge with $\theta_S = 1$, 4 Mo atoms per unit cell, and excluded any dispersion corrections. This modified model system resulted in the alternating configuration being 0.93 eV more stable than the monomer configuration.

Table S4. Comparison of different S monomer/dimer configurations on the S-edge of bulk MoS_2 with $\theta_S = 1$. All energies are with respect to the corresponding monomer configuration. Note that the 4 Mo unit cell has 50%/50% monomers/dimers whereas the 3 Mo unit cell has 67%/33% monomers/dimers. The 4 Mo unit cell has the bottom 3 layers fixed in their crystallographic positions.

	Full monomer	Alternating monomer/dimer
4 Mo unit cell	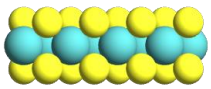	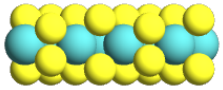
	0 eV	0.17 eV
3 Mo unit cell	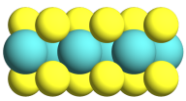	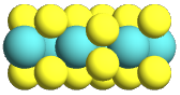
	0 eV	0.11 eV

As noted by Schweiger et al.,[6] the S-edge with 50% S-coverage is most stable with a zig-zag configuration of S adatoms. Due to the odd number of Mo atoms in the simulation unit cell, the structure shown in Table 3 has a "nearly" zig-zag structure. On an eV/atom basis, the two structures shown in Table S5 are nearly identical in energy, and when scaled up to 69 atoms, the energy difference is a mere 0.01 eV.

Table S5. Comparison of zig-zag configurations on the S-edge with 50% S-coverage using a 3 Mo unit cell and a 4 Mo unit cell. The energies are those reported from VASP.

Structure	Image	eV/atom	eV (69 atoms)
4 Mo unit cell (full zig-zag)	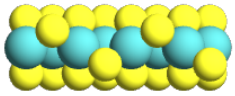	-7.3387	-506.37
3 Mo unit cell (nearly zig-zag)	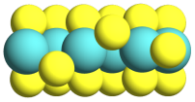	-7.3388	-506.38

Mo-S Bond Energy: Dispersion-Corrections

As shown in Table 2, it was found that S-adsorption is continuously exothermic from $\theta_S = 0 - 1$ on the Mo-edge, which was only found with the inclusion of dispersion corrections. To confirm that this trend is not restricted to just the D3(BJ) dispersion-correction scheme, we also investigated S-adsorption on the Mo-edge using the dDsC scheme (at the PBE-dDsC optimized geometry of a = 3.18 Å, $c/2$ = 6.31 Å, ξ = 0.124). As is shown in Figure S3, the trend remains unchanged when using a different dispersion-correction model (the S-adsorption energy is simply the negative of the Mo-S bond energy).

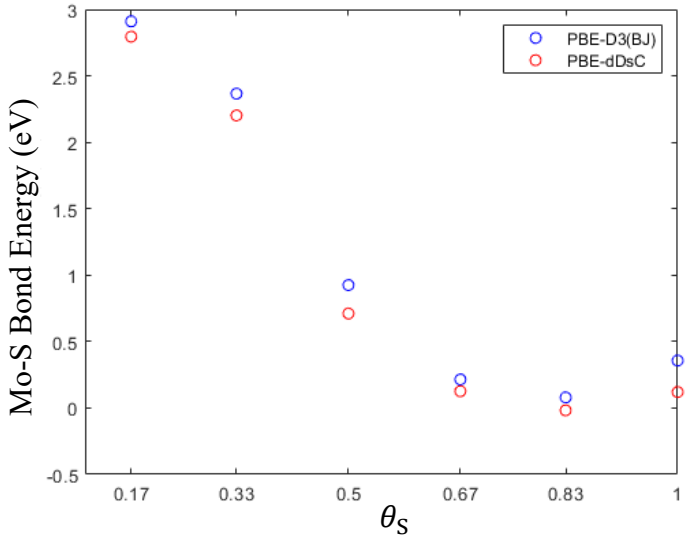

Figure S3. Mo-S bond energy (electronic energy difference) on the Mo-edge as a function of θ_S using PBE-D3(BJ) (blue circles) and PBE-dDsC (red circles).

Additional Mo-S Bond Energies

The Mo-S bond energies reported in Figure 6 are for the most stable structures shown in the $\theta_H = 0$ column of Table 2 and Table 3. There are some edge sites for which there are multiple chemically unique S sites that can be desorbed, resulting in multiple Mo-S bond energies for a given θ_S value depending on which site is investigated. Table S6 highlights these additional Mo-S bond energies alongside those that were reported in Figure 6. Visualizations corresponding to the initial and final states of the MoS_2 edge sites are shown.

Table S6. Mo-S bond energies as a function of S-coverage, defined as the energy to desorb a single S adatom in the presence of H_2 to form H_2S.

θ_S	Edge	ΔE (eV)	$\Delta G^\circ_{1000\,K}$ (eV)	Initial edge site	Final edge site
0.17	Mo-edge	2.91	2.58	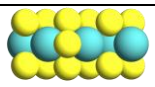	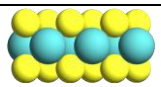
	S-edge	3.84	3.48	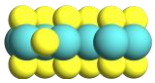	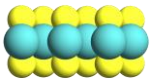
0.33	Mo-edge	2.37	2.03	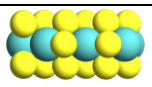	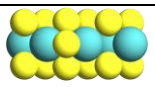
	S-edge	3.61	3.32	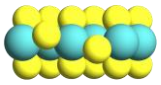	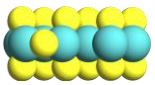
0.5	Mo-edge	0.93	0.57	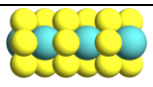	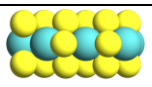
	S-edge	2.31	1.83	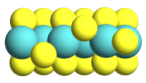	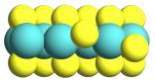
0.67	Mo-edge	0.21	-0.32	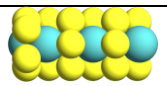	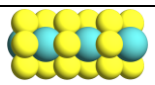

		0.68	0.14	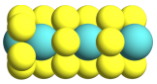	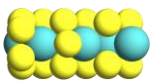
	S-edge	0.98	0.60	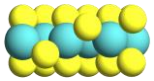	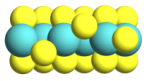
		2.61	2.20	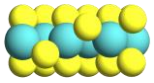	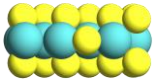
0.83	Mo-edge	0.08	-0.12	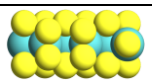	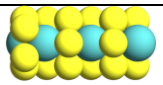
		1.90	1.70	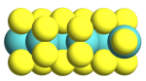	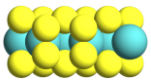
	S-edge	1.05	0.66	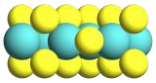	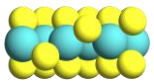
		3.21	2.82	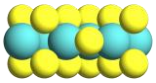	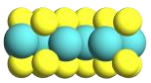
1	Mo-edge	0.36	0.24	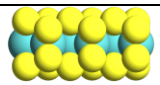	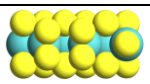
	S-edge	0.94	0.52	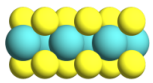	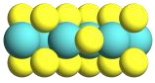

Summarized Methodology

Since there are many steps involved in generating the *ab initio* thermodynamic phase diagrams, this section serves to summarize the implemented workflow:

Performing the DFT Calculations:

1. Optimize lattice constants (a, c) and internal degrees of freedom (ζ) for MoS_2
2. Construct surface slab model of the (100) surface
3. Add S adatoms to Mo- and S-edges to generate structures with coverages of $\theta_S = 0 - 1$
4. Compute the DFT electronic energies for each configuration and keep the lowest energy structure at each value of θ_S
5. Sequentially add H adatoms to the Mo- and S-edges from Step 4 to generate coverages of $\theta_H = 0 - 1$, keeping the lowest energy structure at each new θ_H
6. At this point, the structures present in Table 2 and Table 3 are generated, and a corresponding $E_{MoS_xH_y}$ is computed for each structure
7. Compute the vibrational frequencies of S* for $\theta_S = 0 - 1$ and $\theta_H = 0$
8. Compute the coverage-independent vibrational frequencies of H*

Generating the Phase Diagrams:

1. Pick a fixed temperature T
2. Using the harmonic approximation and the vibrational frequencies from Step 7/8, compute $F_{S^*}^{vib}(T)$ and $F_{H^*}^{vib}(T)$

3. Compute $F_{\mathrm{MoS}_x\mathrm{H}_y}(T)$ for each structure
4. Assume a range of values for $\Delta\mu_{\mathrm{S}^*}$ and $\Delta\mu_{\mathrm{H}^*}$ (the independent variables) and use this with $F_{\mathrm{MoS}_x\mathrm{H}_y}(T)$ to generate $\Phi_{\mathrm{MoS}_x\mathrm{H}_y}$ (the dependent variable) for each edge structure
5. Make a contour plot that shows the edge structure with the lowest $\Phi_{\mathrm{MoS}_x\mathrm{H}_y}$ at a given $\Delta\mu_{\mathrm{S}^*}$ and $\Delta\mu_{\mathrm{H}^*}$
6. To include the corresponding fugacities on the contour plot, use the already generated mesh of $\Delta\mu_{\mathrm{S}^*}$ and $\Delta\mu_{\mathrm{H}^*}$ to generate the equivalent axes in terms of fugacities via $f_i/f^\circ = e^{(\mu_i - \mu_i^\circ)/k_\mathrm{B}T}$
7. Repeat process for different temperatures as desired

Phase Diagrams from 300 K – 1000 K

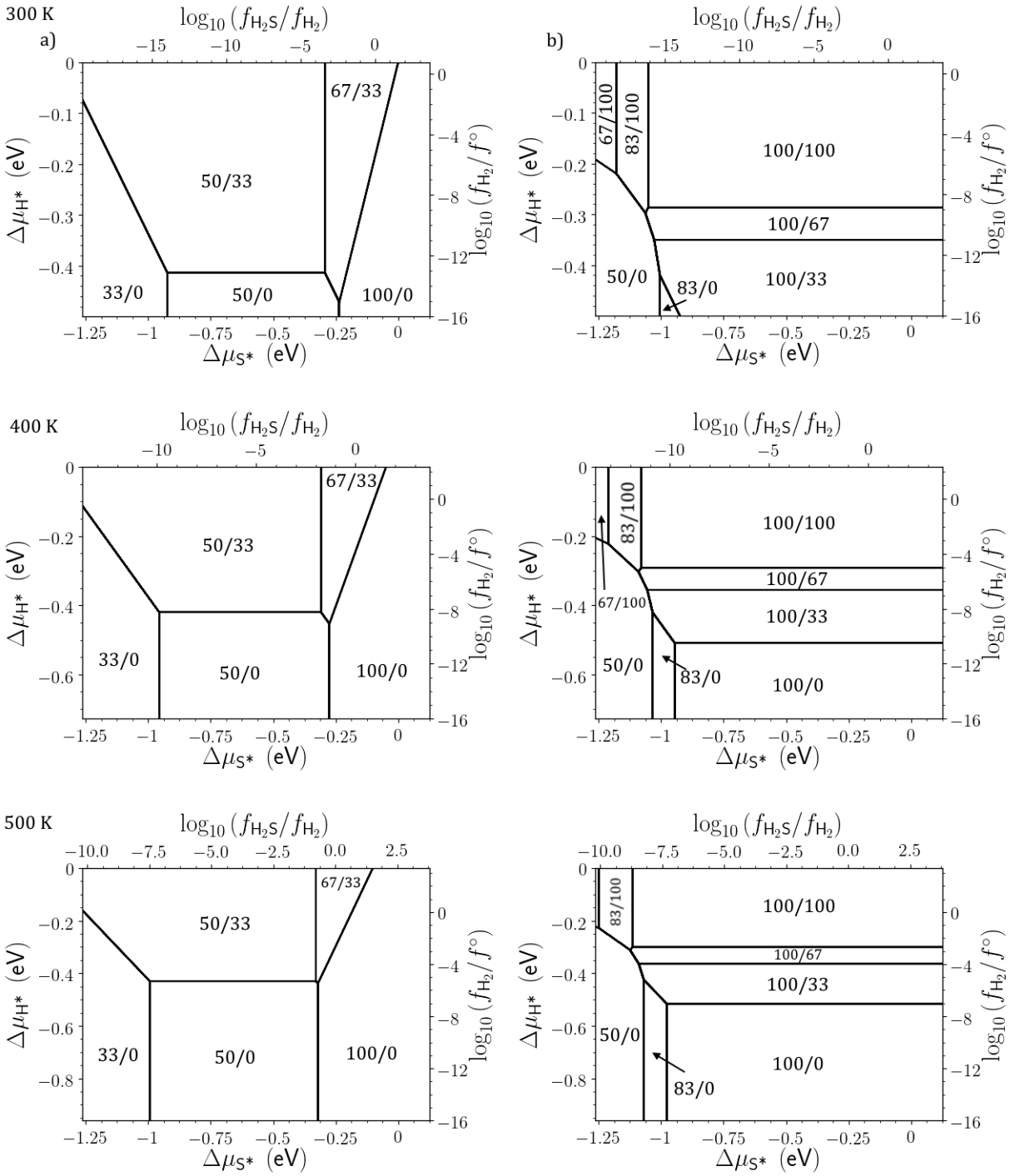

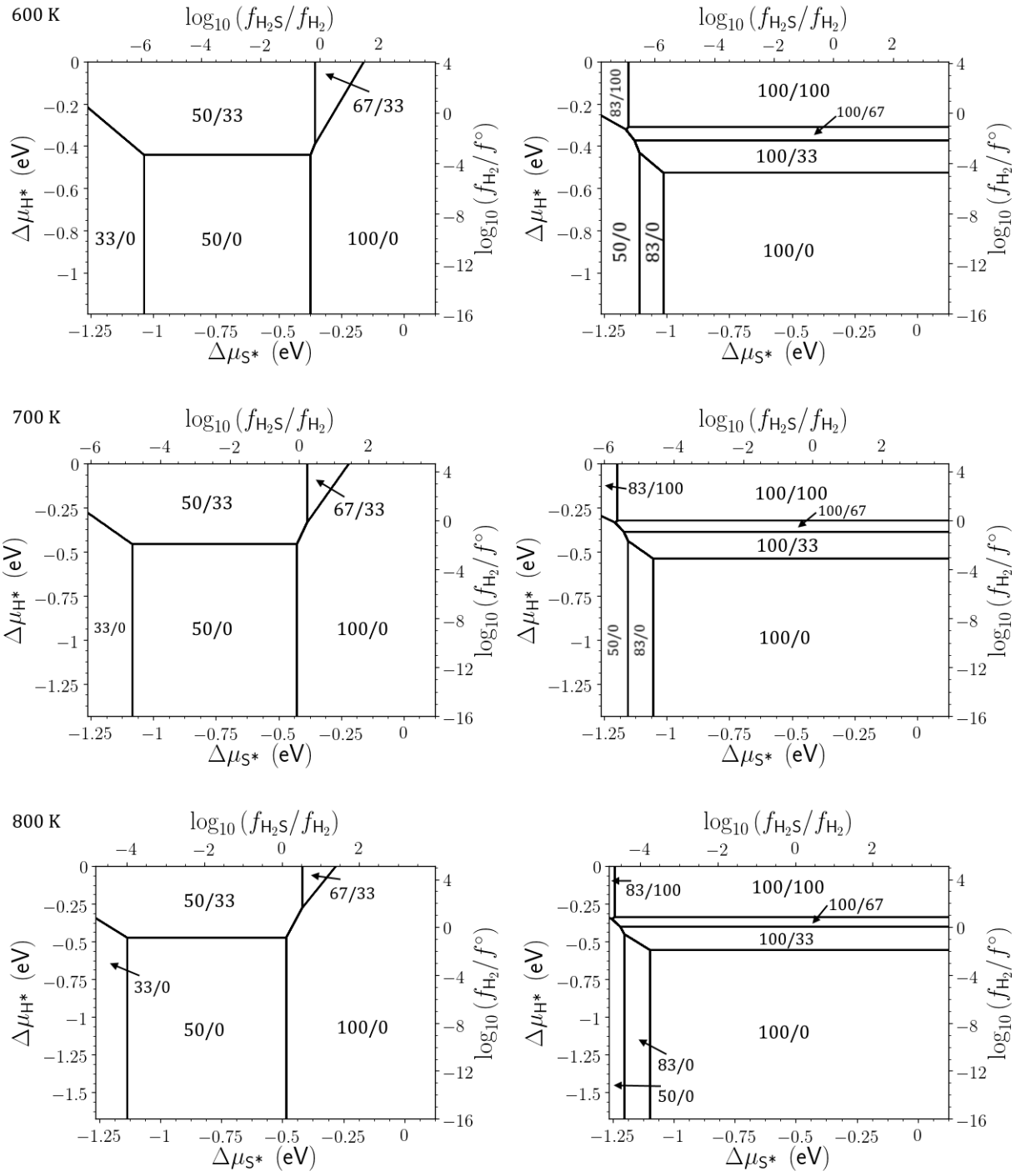
600 K
700 K
800 K
$\log_{10}(f_{H_2S}/f_{H_2})$
$\Delta\mu_{H^*}$ (eV)
$\Delta\mu_{S^*}$ (eV)
$\log_{10}(f_{H_2}/f^\circ)$
50/33
67/33
33/0
50/0
100/0
83/100
100/100
100/67
100/33
50/0
83/0

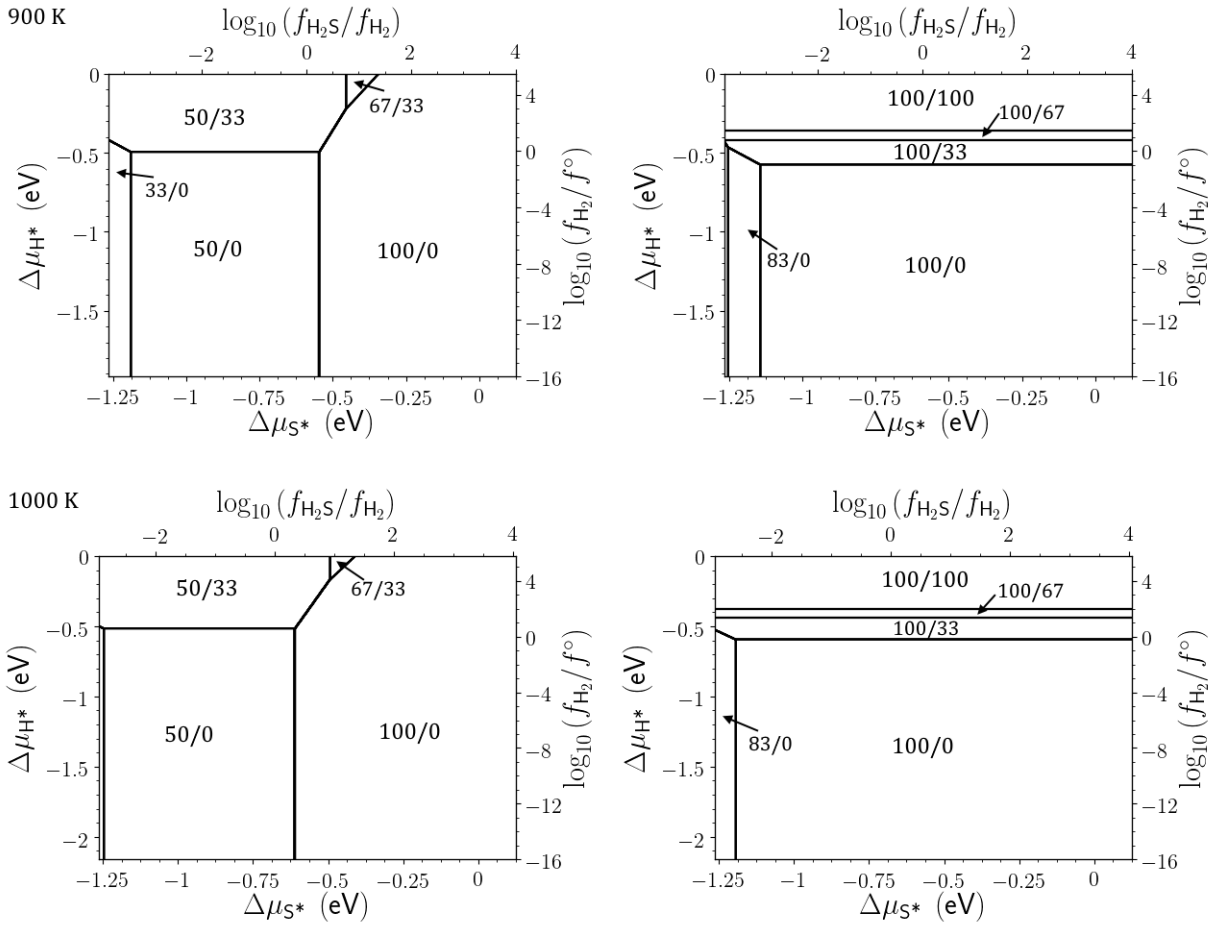

Figure S4. Calculated MoS_2 surface phase diagrams showing the most thermodynamically stable edge configurations from 300 K – 1000 K as a function of the chemical potential of adsorbed sulfur $\Delta\mu_{S^*}$, chemical potential of adsorbed hydrogen $\Delta\mu_{H^*}$, and fugacities f_i of gaseous H_2S and H_2. The reference fugacity f° is 1 bar. (a) Mo-edge. (b) S-edge.

References

(1) Bronsema, K. D.; De Boer, J. L.; Jellinek, F. On the Structure of Molybdenum Diselenide and Disulfide. *ZAAC - J. Inorg. Gen. Chem.* **1986**, *540* (9–10), 15–17.

(2) Downs, R. T.; Hall-Wallace, M. The American Mineralogist Crystal Structure Database. *Am. Mineral.* **2003**, *88* (1), 247–250.

(3) Raybaud, P.; Hafner, J.; Kresse, G.; Kasztelan, S.; Toulhoat, H. Ab Initio Study of the H_2–H_2S/MoS_2 Gas–Solid Interface: The Nature of the Catalytically Active Sites. *J. Catal.* **2000**, *189* (1), 129–146.

(4) Prodhomme, P. Y.; Raybaud, P.; Toulhoat, H. Free-Energy Profiles along Reduction Pathways of MoS_2 M-Edge and S-Edge by Dihydrogen: A First-Principles Study. *J. Catal.* **2011**, 280, 178–195.

(5) Hinnemann, B.; Nørskov, J.; Topsøe, H. A Density Functional Study of the Chemical Differences between Type I and Type II MoS_2-Based Structures in Hydrotreating Catalysts. *J. Phys. Chem. B* **2005**, *109* (6), 2245–2253.

(6) Schweiger, H.; Raybaud, P.; Kresse, G.; Toulhoat, H. Shape and Edge Sites Modifications of MoS_2 Catalytic Nanoparticles Induced by Working Conditions: A Theoretical Study. *J. Catal.* **2002**, *207* (1), 76–87.